中国激光

飞秒激光光丝电学特性实验及模型分析

刘晓松[1]，裴哲浩[1*]，陈维江[2]，张乔根[1]，傅中[3]，杜斌[4]

[1]西安交通大学电气工程学院电力设备电气绝缘国家重点实验室，陕西 西安 710049；

[2]国家电网有限公司，北京 100031；

[3]国网安徽省电力有限公司电力科学研究院，安徽 合肥 230001；

[4]合肥工业大学电气与自动化工程学院，安徽 合肥 230009

摘要 飞秒激光在高压放电、电场测量等领域中有广阔的应用前景，准确测量飞秒激光的相关电学参数是各领域中飞秒激光应用的前提。基于激光电学特性实验得到了光丝通道在恒定电场下的电流特征，通过电路仿真得出了实验电路的等效元件参数，并通过仿真结果与实验条件联立的方法逆推得出以下结论：对于飞秒激光经过辅助聚焦后形成的光丝，其在实验电路中的等效电阻随光丝传播距离的增加呈现先减小后增大的变化趋势。2.7 mJ飞秒激光光丝在通过5 m焦距透镜后，贯穿2.5 cm放电间隙。在这个过程中，当光丝传播距离为473.6～501.6 cm时，等效电阻为457.5～9122.5 kΩ。所提分析方法能够表征具体激光能量和聚焦距离下的飞秒激光光丝的电学特性，研究结果为飞秒激光在高电压领域中的应用提供了参数支持。

关键词 测量；飞秒激光；光丝；激光能量；聚焦距离；等效电阻；电学特性

中图分类号 TN241 **文献标志码** A **DOI**：10.3788/CJL220711

1 引 言

飞秒激光在空气中通过克尔自聚焦效应形成光丝，经过自聚焦后的光强度可达10^{18}～10^{22} W/cm^2[1-3]，其强度超过了原子内部的库仑场，利用聚焦后的飞秒激光脉冲可将电子从原子的束缚中剥离出来，从而形成等离子体。飞秒激光成丝过程存在诸多复杂的非线性过程，如自聚焦、光致电离、自相位调制、自陡峭、衍射及散焦等[4-7]。其成丝特性在高电压领域中有广阔的应用前景[8-11]。

将飞秒激光应用在其他领域需要准确测量飞秒激光的各项参数。飞秒激光脉冲种类繁多，其测量技术始终在快速变化和发展[12-13]。通过现有光学观测手段可以获得飞秒激光成丝后不同位置的光丝随时间的演化特性。段作梁等[14]观测到飞秒激光脉冲在大气传输过程中的光束截面从双丝演变为单丝并最终消散的过程，并测量了光丝的长度。李永亮等[15]采用激光束照射漫反射靶，利用电荷耦合器件(CCD)相机对靶上激光光斑进行成像，获得了激光在长距离成丝时不同位置处的光丝截面图像及对应光丝直径。Thiyagarajan等[16]通过增强电荷耦合器件(ICCD)观测到在不同时间尺度下同一位置光丝截面上的光丝直径变化趋势，并得出光丝在空气中的寿命。上述学者的研究方法较好地测量了光丝尺寸、光丝数量及寿命等光学参数，但不能获得光丝的电学特性。

飞秒激光电学特性主要表现为光丝通道的电阻特性。对于飞秒激光引起或诱导的各类放电，放电通道的电流特性与飞秒激光光丝的电阻特性密切相关，有必要采用合理的研究方法对光丝通道电阻特性进行研究。飞秒激光具有功率高、持续时间短、通道半径小等特点，其光丝的电阻特性测量缺乏较好的实验方法。李玉同[17]利用诺马斯基干涉仪对飞秒激光的光丝等离子体进行了诊断，得到了不同延迟时间下的激光等离子体阴影图和干涉图。Chizhov等[18]利用迈克耳孙干涉仪对高压空气中飞秒激光的光丝等离子体进行了研究，结果显示，随着空气压强的增加，电子复合速率单调增加，在3～4个大气压内，初始电子密度急剧增大，同时光丝直径显著减小。Point等[19]利用马赫-曾德尔干涉仪研究了飞秒激光脉冲的聚焦条件、偏振及波长等实验参数对光丝等离子体的影响，结果表明，在紧聚焦的情况下，光丝等离子体产生了一个冲击波，由此产生的低密度通道的寿命超过了90 ms。以上学者针对飞秒激光光丝等离子体特性进行了研究，表征了光丝的通流能力并定性表征了光丝的等效电阻，但不能量化光丝的等效电阻。张喆等[20]通过将光丝与电极接触，测量了电路中的总阻抗，进而推算出光丝等效电

收稿日期：2022-03-28；**修回日期**：2022-05-05；**录用日期**：2022-05-16；**网络首发日期**：2022-05-26

基金项目：国家电网公司科技项目(52120519003H)

通信作者：*peizhehao@126.com

阻，得到了能量为48 mJ的飞秒激光经过2 m焦距透镜辅助聚焦后形成的光丝段的等效电阻，发现光丝焦点处的等效电阻为最小值，其电阻率为$3.6\times10^{-2}\ \Omega/cm$。但该实验模型未考虑光丝与电极间的等效电容，这会导致在实验结果分析过程中忽略电容对回路电流波形的影响，造成光丝等效电阻的计算误差，因此还需要准确考虑实验电路中所有等效元件对测量结果的影响。

针对上述测量难题，本文搭建了带有光丝通道的电学回路并对回路电流进行了测量，得到了飞秒激光经过聚焦后形成的光丝段在恒定电场下产生的电流波形，并根据实验平台构建了仿真电路，得出了电路中的所有等效元件参数，最终通过实验数据反推出光丝的电学特性。

2　实验布置

实验采用一对平行铜板，铜板半径为10 cm，厚度为1 cm，间隙宽度为2.5 cm，板电极中心圆孔的直径为5 mm，保证光丝不与圆孔接触，实验布置如图1所示，其中U_d为外施电压，C为充电电容，$I(t)$为回路电流。飞秒激光被反射镜组准直后垂直射向板电极圆心。板电极前方的聚焦透镜对飞秒激光起辅助聚焦作用，激光聚焦透镜的焦距为1 m和5 m。通过使用不同焦距的聚焦透镜并改变透镜与板的距离(x_L)，研究了不同聚焦距离下光丝在不同位置处的电学特性。

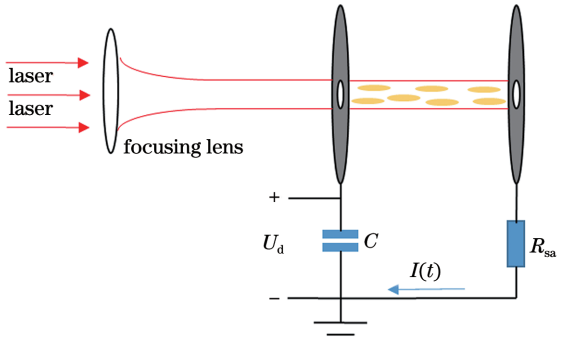

图1　激光电学特性实验布置图

Fig. 1　Layout of laser electrical characteristic experiment

板间施加直流电压以产生均匀电场，并串接采样电阻(R_{sa})，从而构成实验回路。R_{sa}的值为50 Ω，通过示波器连接高压表笔，并将高压表笔接在采样电阻两端，从而得到采样电阻的电压波形。高压表笔的测量带宽为150 MHz，示波器的采样点时间间隔为10 ps，满足被测波形对测量设备带宽的要求。计算了回路电流波形。

3　实验结果

根据图1所示实验装置图，2.7 mJ能量的激光经过1 m焦距的聚焦透镜后，传播98 cm到达板-板间隙，激光中心波长为800 nm、脉冲宽度为56 fs、重复频率为10 Hz。通过改变板间外施电场，研究了由光丝引起的回路瞬时电流幅值的变化情况，结果如图2所示。

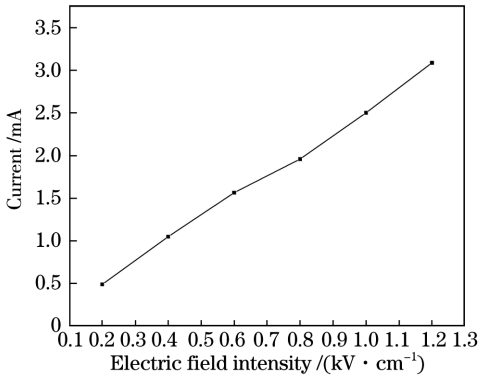

图2　回路电流幅值与板间外施电场的关系

Fig. 2　Relationship between loop current amplitude and applied electric field between plates

如图2所示，回路电流幅值和板间外施电场呈近似线性关系，可以固定板间外施电场并进行下一步研究。当板间外施电场强度为0.8 kV/cm时，在激光能量从2 mJ变化到30 mJ的过程中，观测到的回路电流幅值变化情况如图3所示。可以看到，回路电流幅值随激光能量的增加呈近似线性增加。飞秒激光能量的增大会影响光丝通道内部的电离特性，使得飞秒激光成丝后产生更多自由电子，从而改变光丝通道的等效电阻。

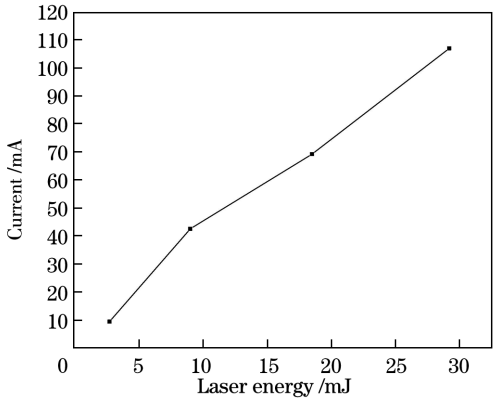

图3　回路电流幅值与激光能量关系

Fig. 3　Relationship between loop current amplitude and laser energy

基于板间外施电场和激光能量对回路电流的影响规律，接下来研究x_L与回路电流的关系。当板-板间隙宽度为2.5 cm、板间电场强度为0.8 kV/cm、激光能量为2.7 mJ时，1 m焦距透镜下的光丝电流幅值随x_L的变化情况如图4所示。

如图4所示，光丝电流幅值随x_L的变化明显并且呈近似高斯分布。由于焦距较短，1 m焦距的透镜在实验中不利于获取成丝状态恒定的光丝。

选择焦距为5 m的聚焦透镜开展实验，在该透镜下光丝始终为多丝状态，图5为CMOS相机(CMOS，

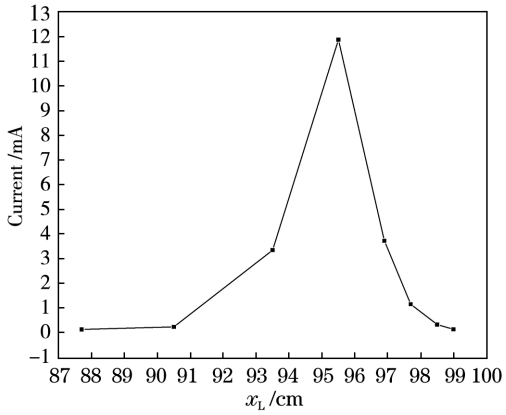

图 4 回路电流幅值与 1 m 焦距透镜下的 x_L 的关系

Fig. 4 Relationship between loop current amplitude and x_L under 1 m focal length lens

互补金属氧化物半导体)拍摄到的不同位置处的光丝截面图。保持其他条件不变,5 m 焦距透镜下的回路电流幅值随 x_L 的变化如图 6 所示。对比图 6 和图 4 可以发现:采用 1 m 焦距透镜和 5 m 焦距透镜时,光丝在同一电路下产生的回路电流幅值相近,均为 11~12 mA;相较于 1 m 焦距透镜条件下,5 m 焦距透镜对激光的聚焦作用使激光在空气中传播时形成的光丝直

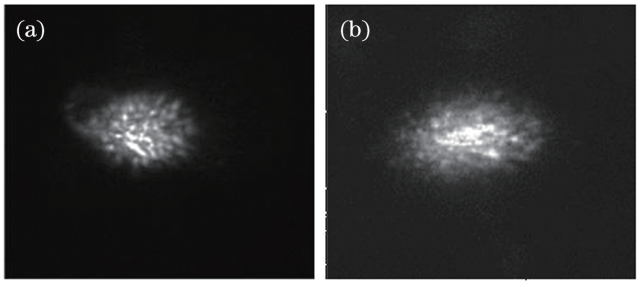

图 5 飞秒激光光丝的截面观测图。(a)与聚焦透镜的距离为 4.95 m;(b)与聚焦透镜的距离为 5.18 m

Fig. 5 Cross section views of femtosecond laser filaments. (a) Distance from focusing lens is 4.95 m; (b) distance from focusing lens is 5.18 m

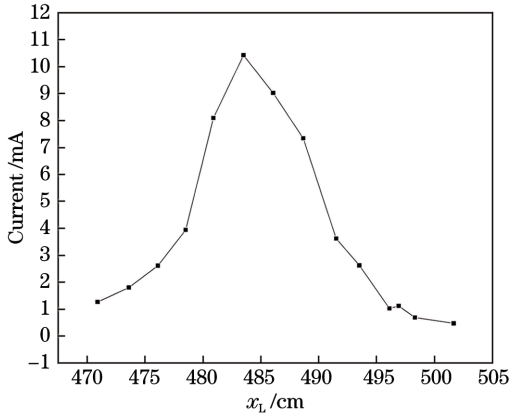

图 6 回路电流幅值与 5 m 焦距透镜下的 x_L 的关系

Fig. 6 Relationship between loop current amplitude and x_L under 5 m focal length lens

径较大、长度较长,电离区域激光的平均峰值功率较低,电离程度相对较弱,所以电流幅值较低,光丝电学特性随 x_L 的变化较缓慢。由图 6 可知,当 5 m 焦距透镜下的 x_L 为 480~490 cm 时,光丝电流幅值较高且恒定。

4 光丝电学特性实验的等效电路模型

为了进一步分析获得的光丝的电学特性,根据图 1 搭建了基于 PSCAD 软件的实验仿真电路,如图 7 所示,其中 E_c 为外施电压,E_{r2} 为采样电阻电压,R 为电源内阻,I_a 为回路电流,I_b 为板板间隙电容电流,I_c 为光丝通路电流,R_a 为空气环等效电阻,C_a 为空气环等效电容。

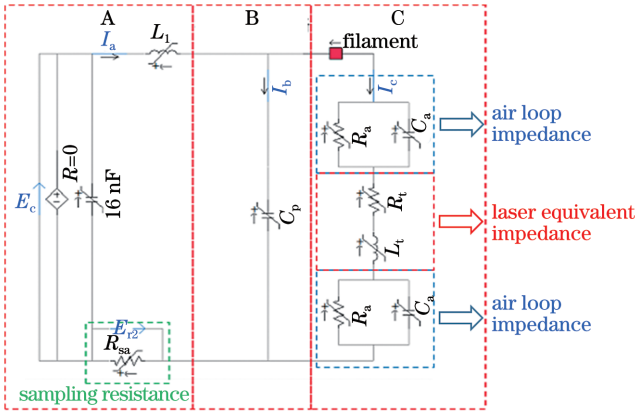

图 7 光丝电学特性实验的等效电路模型

Fig. 7 Equivalent circuit model of filament electrical characteristics experiment

图 7 电路分为充电电路(A)、板-板等效支路(B)和光丝等效支路(C)三部分。充电电路包括直流电源、充电电容(16 nF)和线路等效电感(L_1)。板-板等效支路由两个板电极自身的等效电容(C_p)构成。光丝等效支路包括光丝和板间的空气环阻抗(C_a 和 R_a)及光丝等效阻抗。光丝等效阻抗由光丝等效电阻 R_t 与等效电感 L_t 构成,在光丝等效支路设置断路器,使其在光丝入射的 1 μs 后导通,用于模拟激光入射板-板间隙的瞬态过程。其中线路等效电感 L_1 的参数值为 1440 nH,由实验波形的振荡特性确定。根据板电极实际尺寸和两板间隙宽度,建立有限元仿真模型,确定板-板等效支路中的 C_p 为 19.44 nF。光丝等效支路的 C_a、R_a、R_t、L_t 需要通过分析实验波形来确定。

5 光丝电学特性分析方法

飞秒激光光丝在空气中的寿命极短(无外施电场条件下小于 10 ns),并且光丝轴向等离子体密度分布不均匀,同时存在聚焦后的电离过程与电离引起的散焦过程,二者随传播时间的增加呈振荡变化。根据光丝性质,假设光丝等效电阻表达式为振荡上升的指数函数,结合实验中采样电阻的电压波形,假设其表达式为

$$R_t = R_{laser} \times e^{4\times10^6\times t} + 0.5 \times R_{laser} \times \sin(1.7\times10^7\times t + 180) \times e^{2.5\times10^6\times t}, \quad (1)$$

式中：R_{laser}为光丝初始电阻；t为时间。通过参数调试，得出 C_a=0.5 pF、R_a=10 kΩ、L_t=10 nH、R_{laser}=800 kΩ时仿真电路中采样电阻的电压波形，与实验实测波形进行对比，结果如图 8 所示。实验实测波形是激光能量为 2.73 mJ、聚焦透镜焦距为 5 m、x_L为 493.5 cm 时的采样电阻电压波形。

如图 8 所示，模拟波形较好模拟了实测波形中的首次上升沿波形特征，对后续波形也有较好的跟随性，与实测波形振荡周期相近，幅值相近。其中实测波形 200 μs 后的小幅振荡是由背景噪声引起的。通过改变 R_{laser}的值观测模拟波形的变化特性，认为采用前文中的 C_a、R_a和 L_t值时产生的模拟波形能够较好表征实测波形的特征。

基于式(1)中 R_t的表达式，建立仿真电路中 R_{sa}电压波形和光丝初始电阻 R_{laser}的关系，结果如图 9 所示。图 9 为基于仿真电路复现出的实验波形，实验实测数据与仿真电路中具体元件参数下的仿真结果相对应。将

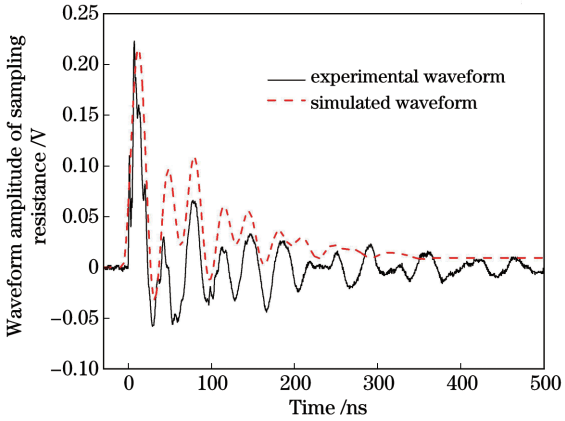

图 8　模拟波形与实测波形的对比

Fig. 8　Comparison between simulated waveform and measured waveform

图 9 中 R_{sa}电压波形幅值与 R_{laser}的对应关系绘制成曲线，如图 10 所示。图 10 清晰表示了具体光丝电阻初始值 R_{laser}所对应的 R_{sa}电压波形幅值，将其与实验中 R_{sa}实测波形幅值进行对比，得出 2.7 mJ 激光在 5 m 焦距透镜下的光丝在电路中的等效电阻与 x_L的关系，如图 11 所示。

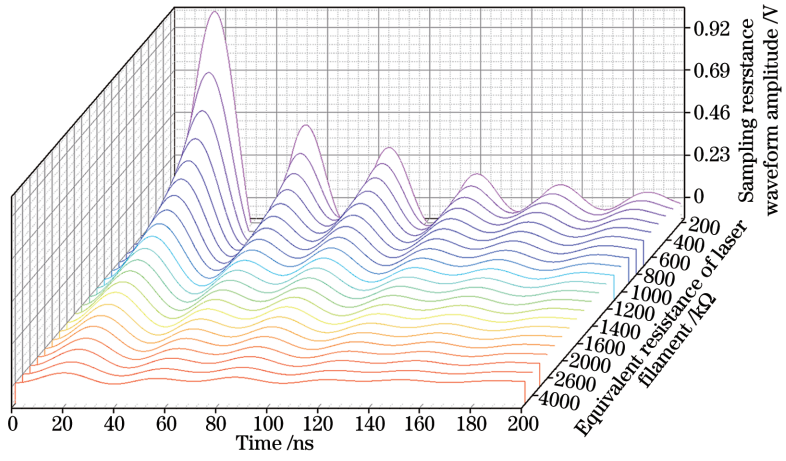

图 9　采样电阻波形与光丝等效电阻关系

Fig. 9　Relationship between sampling resistance waveform and filament equivalent resistance

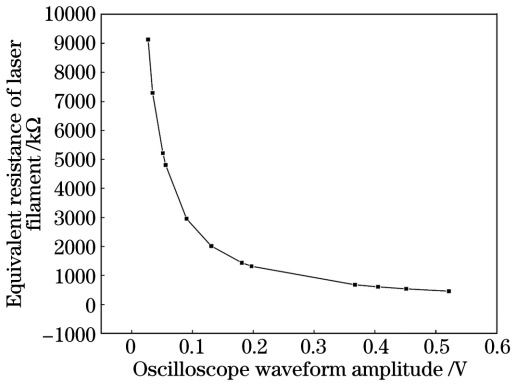

图 10　回路电流幅值与光丝等效电阻关系

Fig. 10　Relationship between loop current amplitude and filament equivalent resistance

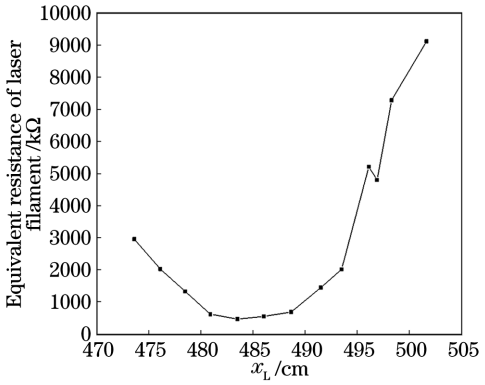

图 11　光丝等效电阻与 x_L的关系

Fig. 11　Relationship between equivalent resistance of filament and x_L

如图 11 所示，飞秒激光经过辅助聚焦后形成的光丝等效电阻 R_t随 x_L的增加呈先减小后增大的变化趋势，其最低值为 457.50 kΩ，对应聚焦距离为 483.5 cm。光丝低阻值通道(457.50～676.25 kΩ)长度为 7.75 cm

(480.90～488.65 cm)。当x_L大于480.90 cm时,由于等离子散焦效应,光丝通道等离子体密度随x_L的增加而急剧下降,对应的光丝等效电阻R_t急剧上升。实验中测量到的R_t最高值为9122.5 kΩ,在成丝段末端,对应聚焦距离为501.6 cm。

6 结 论

通过搭建激光电学特性实验平台,结合仿真电路,对飞秒激光光丝的电学特性进行了研究,得到了飞秒激光光丝在均匀电场中的电流特征及聚焦透镜与板-板间隙距离改变时光丝通道在电路中的等效电阻变化规律。具体结论如下:

1)外施电场和激光能量对光丝等效电阻具有显著影响,在0.2～1.2 kV/cm外施电场下和2～30 mJ激光能量内,光丝等效电阻随着外施电场或激光能量的增加均近似线性减小。

2)光丝等效电阻随聚焦透镜与板-板间隙距离的增加呈先减小后增大的变化趋势。在5 m焦距透镜下,当2.7 mJ能量的激光光丝贯穿间距为2.5 cm、光丝轴向电场强度为0.8 kV/cm的间隙时,对应光丝传播距离在473.6～501.6 cm范围的等效电阻为457.5～9122.5 kΩ。

3)基于光丝电学特性的等效电路模型,通过PSCAD软件建立了仿真电路。建立了实验电路中光丝通道的等效电阻表达式,得到了光丝等效电路元件参数与实测数据的对应关系,为光丝电学特性的测量提供了有效方法与参数支持。

参 考 文 献

[1] 彭翰生. 超强固体激光及其在前沿学科中的应用[J]. 中国激光, 2006, 33(6): 721-729.
Peng H S. Ultraintense solid-state lasers and applications to the frontiers of sciences[J]. Chinese Journal of Lasers, 2006, 33(6): 721-729.

[2] 冯玺, 张兆伟. 基于差频技术的宽谱中红外飞秒激光的产生[J]. 中国激光, 2022, 49(1): 0101018.
Feng X, Zhang Z W. Broadband mid-infrared light based on difference frequency generators[J]. Chinese Journal of Lasers, 2022, 49(1): 0101018.

[3] 冯天利, 商景诚, 李涛. 基于双光成丝过程的光参量啁啾脉冲放大器前端[J]. 中国激光, 2022, 49(7): 0708002.
Feng T L, Shang J C, Li T. Front-end of optical parametric chirped-pulse amplifier based on dual laser filamentation[J]. Chinese Journal of Lasers, 2022, 49(7): 0708002.

[4] 赵其锴, 丛振华, 刘兆军, 等. 百微焦飞秒光纤啁啾脉冲放大激光系统[J]. 中国激光, 2021, 48(7): 0701001.
Zhao Q K, Cong Z H, Liu Z J, et al. Hundred microjoule femtosecond fiber chirped pulse amplification laser system[J]. Chinese Journal of Lasers, 2021, 48(7): 0701001.

[5] 张旋, 王铁军, 郭豪, 等. 脉宽依赖的飞秒激光成丝钳制光强的研究[J]. 中国激光, 2019, 46(9): 0901005.
Zhang X, Wang T J, Guo H, et al. Pulse-duration-dependent clamping intensity in femtosecond laser filament[J]. Chinese Journal of Lasers, 2019, 46(9): 0901005.

[6] 况琪, 申雄, 徐艺林, 等. Dense-1D-U-Net: 用于自参考光谱干涉飞秒脉冲相位测量[J]. 中国激光, 2022, 49(9): 0904002.
Kuang Q, Shen X, Xu Y L, et al. Dense-ID-U-net: encoder-decoder networks for self-referenced spectral interferometry[J]. Chinese Journal of Lasers, 2022, 49(9): 0904002.

[7] 陈晓义, 段亚轩, 王拯洲, 等. 基于多步相位恢复的激光远场焦斑测量方法[J]. 中国激光, 2022, 49(7): 0704002.
Chen X Y, Duan Y X, Wang Z Z, et al. Laser far-field focal spot measurement method based on multistep phase retrieval[J]. Chinese Journal of Lasers, 2022, 49(7): 0704002.

[8] 王光昶, 郑志坚, 谷渝秋, 等. 超热电子输运背向光辐射的实验研究[J]. 物理学报, 2008, 57(8): 5117-5122.
Wang G C, Zheng Z J, Gu Y Q, et al. Experimental study of optical radiation of hot electrons transport in targets at the rear-side radiation[J]. Acta Physica Sinica, 2008, 57(8): 5117-5122.

[9] Cheng C R, Xu X F. Mechanisms of decomposition of metal during femtosecond laser ablation[J]. Physical Review B, 2005, 72(16): 165415.

[10] 岳帅英, 林晨, 高军毅. 飞秒激光空气等离子体通道的吸收和辐射特性[J]. 光学学报, 2010, 30(1): 241-245.
Yue S Y, Lin C, Gao J Y. Absorption and emission characteristics of plasma channel produced by femtosecond laser pulse in air[J]. Acta Optica Sinica, 2010, 30(1): 241-245.

[11] 王铁军, 陈娜, 郭豪, 等. 飞秒强激光大气遥感新技术的原理和研究进展[J]. 激光与光电子学进展, 2022, 59(7): 0700001.
Wang T J, Chen N, Guo H, et al. Principle and research progress of atmospheric remote sensing by intense femtosecond lasers[J]. Laser & Optoelectronics Progress, 2022, 59(7): 0700001.

[12] 刘岩. 空气中飞秒激光成丝过程中的激光脉冲诊断方法研究[D]. 天津: 南开大学, 2011.
Liu Y. The pulse characterization during femtosecond laser filamentaion in air[D]. Tianjin: Nankai University, 2011.

[13] 王玉英. 超短脉冲激光器及其应用[J]. 光机电信息, 2006, 23(3): 21-28.
Wang Y Y. Ultrashort pulse laser and its application[J]. OME Information, 2006, 23(3): 21-28.

[14] 段作梁, 陈建平, 方宗豹, 等. 1 kHz飞秒激光脉冲在空气中传输成丝的演化过程[J]. 物理学报, 2004, 53(2): 473-477.
Duan Z L, Chen J P, Fang Z B, et al. Evolvement of filamentation of femtosecond laser pulses of a kHz repetition rate propagating in air[J]. Acta Physica Sinica, 2004, 53(2): 473-477.

[15] 李永亮, 姜会林. 高功率脉冲激光的远场能量密度分布测试方法研究[J]. 光子学报, 2009, 38(5): 1274-1276.
Li Y L, Jiang H L. Detection methods of far-field energy density of the high power pulse laser[J]. Acta Photonica Sinica, 2009, 38(5): 1274-1276.

[16] Thiyagarajan M, Scharer J. Experimental investigation of ultraviolet laser induced plasma density and temperature evolution in air[J]. Journal of Applied Physics, 2008, 104(1): 013303.

[17] 李玉同. 飞秒激光等离子体光学诊断和自生磁场实验研究[D]. 绵阳: 中国工程物理研究院, 2001.
Li Y T. Experimental studies of axial magnetic fields and optical diagnostic of femtosecond laser plasmas[D]. Mianyang: Chinese Academy of Engineering Physics, 2001.

[18] Chizhov P A, Bukin V V, Ushakov A A, et al. Features of the electron density dynamics in the filamentation of femtosecond laser radiation in air at elevated pressure[J]. Quantum Electronics, 2016, 46(4): 332-334.

[19] Point G, Milián C, Couairon A, et al. Generation of long-lived underdense channels using femtosecond filamentation in air[J]. Journal of Physics B: Atomic, Molecular and Optical Physics, 2015, 48(9): 094009.

[20] 张喆, 张杰, 李玉同, 等. 空气中激光等离子体通道导电性能的研究[J]. 物理学报, 2006, 55(1): 357-361.
Zhang Z, Zhang J, Li Y T, et al. Measurements of electric resistivity of plasma channels in air[J]. Acta Physica Sinica, 2006, 55(1): 357-361.

Analysis of Electrical Characteristics of Femtosecond Laser Filaments Through Experiments and Circuit Modeling

Liu Xiaosong[1], Pei Zhehao[1*], Chen Weijiang[2], Zhang Qiaogen[1], Fu Zhong[3], Du Bin[4]

[1]*State Key Laboratory of Electrical Insulation and Power Equipment, School of Electrical Engineering, Xi'an Jiaotong University, Xi'an* 710049, *Shaanxi, China*;

[2]*State Grid Corporation of China, Beijing* 100031, *China*;

[3]*Electric Power Research Institute, State Grid Anhui Electric Power Co. Ltd. , Hefei* 230001, *Anhui, China*;

[4]*School of Electrical Engineering and Automation, Hefei University of Technology, Hefei* 230009, *Anhui, China*

Abstract

Objective Owing to rapid development in laser technology, femtosecond lasers can form plasma filaments of up to 100 m in length. This type of plasma channel has good continuity and relatively low resistivity, which is conducive to guiding long-distance discharge. Therefore, it has broad application prospects in the fields of high-voltage discharge and electric field measurement. Accurate measurement of the relevant parameters of femtosecond lasers is the premise of applying femtosecond lasers in various fields. Existing optical photography methods can accurately measure optical parameters such as the size, number, and service life of the laser filament, but there are few accurate measurement methods for the electrical characteristics of femtosecond laser filaments. The electrical characteristics of laser filaments mainly include the current characteristics and equivalent resistance in an external electric field. Scholars have studied the plasma characteristics of femtosecond laser filaments. This type of research can reflect the current-carrying capacity of the laser filament and qualitatively reflect the equivalent resistance of the laser filament; however, it cannot quantify the equivalent resistance of the laser filament. To measure the femtosecond laser filament equivalent resistance, the measurement principle, measurement accuracy, equivalent circuit, and measurement signal processing of the experimental measurement device must be considered. In this study, a method combining experiments and simulations is used. The experimental data are input into the simulation model, an expression for the femtosecond laser filament equivalent resistance is obtained, and the influence of the laser parameters on the femtosecond laser filament equivalent resistance is analyzed. We hope that this research method can characterize the electrical characteristics of femtosecond laser filaments under specific laser energies and focusing distances to provide parameter support for the application of femtosecond lasers in high-voltage fields.

Methods In this study, the laser filament is injected into a plate-plate gap with a central opening, and a uniform electric field is applied between the plates. The sampling resistance and direct current (DC) voltage source are connected in series between the two plate electrodes to form a discharge circuit. The high-voltage probe is connected through the oscilloscope at both ends of the sampling resistance to obtain the voltage waveform of the sampling resistance. According to the circuit principle, the board-to-board discharge branch in the discharge circuit is equivalent to a discharge branch comprising resistance, inductance, and capacitance. The sampling resistance waveform measured in the experiment is input into the simulation model to obtain the parameter values of each equivalent element in the plate-plate gap discharge branch and the equivalent resistance of the laser filament in a uniform electric field.

Results and Discussions Through the joint analysis of experimental data and simulation, the equivalent circuit of the experimental circuit and the parameters of each element in the equivalent circuit are obtained. The waveform simulated in the equivalent circuit better simulates the wavefront characteristics of the sampled resistance voltage waveform in the experiment and has good follow-up to the subsequent waveform. The oscillation period and amplitude of the simulated waveforms are similar to those of the measured waveforms. According to the experimental data and simulation circuit, the characteristics of the laser filament equivalent resistance are as follows: the applied electric field and laser energy have a significant impact on the laser filament equivalent resistance. Under an applied electric field of 0. 2–1. 2 kV/cm and within 2–30 mJ laser energy, the laser filament equivalent resistance decreases approximately linearly with the increase in the applied electric field or laser energy, as shown in Fig. 2 and Fig. 3. The equivalent resistance of the filament formed by femtosecond laser-assisted focusing in the experimental circuit first decreases and then increases with an increase in the propagation distance of the filament. When the 2. 7 mJ femtosecond laser filament passing through a 5 m focal length lens passes through a 2. 5 cm discharge gap, the equivalent resistance corresponding to the propagation distance of the filament in the range of 473. 6–501. 6 cm is 457. 5–9122. 5 kΩ, as shown in Fig. 11.

Conclusions In this study, a method for measuring the equivalent resistance of femtosecond laser filament is improved, which could give the measurement results more accurate physical significance, and the electrical characteristics of femtosecond laser filaments are studied in combination with a simulation circuit. The current characteristics of the femtosecond laser filament in a uniform electric field and the variation effect of the equivalent resistance of the filament channel in the circuit are obtained when the distance between the focusing lens and plate gap changes. This measurement method considers the influence of stray capacitance, laser filament inductance, and charging capacitance of the measuring device on the measurement results, and it can more accurately measure the equivalent resistance of the laser filament when the laser energy and focusing distance are determined to provide parameter support for the application of femtosecond lasers in the field of high voltage.

Key words measurements; femtosecond laser; filament; laser energy; focusing distance; equivalent resistance; electrical characteristics